Structures 14 (2018) 358–375

Contents lists available at ScienceDirect

Structures

journal homepage: www.elsevier.com/locate/structures

Behaviour of Concrete-filled Double-skin Short Columns Under Compression Through Finite Element Modelling: SHS Outer and SHS Inner Tubes

M.F. Hassanein[a], M. Elchalakani[b,*], A. Karrech[b], V.I. Patel[c], Bo Yang[d,*]

[a] Department of Structural Engineering, Faculty of Engineering, Tanta University, Tanta, Egypt
[b] The School of Civil, Environmental and Mining Engineering at the Faculty of engineering, Computing and Mathematics, The University of Western Australia, Australia
[c] School of Engineering and Mathematical Sciences, La Trobe University, Bendigo, VIC 3552, Australia
[d] School of Civil Engineering, Chongqing University, Chongqing 400045, China

ARTICLE INFO

Keywords:
Concrete-filled tubes
Double-skin
Finite element analysis
Axial compression
Ultimate strength
Design

ABSTRACT

Concrete-filled double-skin tubular (CFDST) columns are formed by sandwiching concrete between two concentric hollow steel tubes. The result is a composite column with the benefits of both steel and concrete properties. When compared to a traditional concrete-filled steel tube (consisting of a single hollow steel tube instead of two), CFDST column is found to have greater axial, flexural and torsional strengths as well as improved strength-to-weight ratios. However, developments in CFDST column configurations can be made by altering the cross-section shape of the steel tubes, which is generally formed from square and circular ones. This paper considers the square CFDST short columns with inner square hollow sections (i.e. SHS outer and SHS inner tubes). This is because; in additional to their advantages shown above, they were seldom considered in literature especially by virtual testing. Accordingly, this paper is devoted for the finite element (FE) modelling of this type of composite columns by using ABAQUS program. Innovatively, this paper, rather than different investigations in literature, uses the most accurate constitutive models of both the cold-formed steel (i.e. Ramberg-Osgood model) and the confined concrete infill in double-skin tubes. Prior to parametric studies, the program has been validated using previous experimental results to ensure that the chosen combination of the materials could provide accurate and reliable results for the proposed models. The paper is then extends through parametric studies to investigate the effects of the key parameters affecting the general behaviour of this column under axial compressive loading, which exceeds the range of materials currently available in the available experiments. The paper additionally explores the effect of the eccentric loads on the behaviour of such columns, rarely done in literature, and comparisons with available theoretical moment-interaction curves have been considered. Overall, this paper provides new results that might aid in widening the practical usage of such column.

1. Introduction

Typical concrete-filled steel tubular (CFST) columns, formed by filling a single hollow steel tube with concrete, have several advantages permitted them to be used extensively in modern high-rise and bridge construction [1]. However, the high concrete content makes the column heavy and hence; it is difficult to improve the strength-to-weight ratio of the column [2]. It has also been found that under compression, the steel tube shares a greater portion of the load than the concrete, due to its higher stiffness under composite action [2]. Additionally, research suggests that the solid concrete core in CFST columns does not significantly contribute to the load-carrying capacity of the column, giving rise to the concept of its replacement by a hollow steel tube [2]. Hence, this leads to the birth of a new type of composite columns; called the concrete-filled double skin steel tubular (CFDST) columns [1]. These CFDST columns are formed by sandwiching concrete between two concentric, hollow steel tubes. These tubes are mostly either circular or square in cross section [3–10], meaning that the columns can be comprised of two circular tubes, two square tubes or one of each; see Fig. 1.

When compared with CFST columns of similar outer dimensions, CFDST columns have been observed to achieve higher axial, flexural and torsional strengths. Consequently, this results in greater strength-to-weight ratios as well as providing a more environmentally sustainable option, given the significant reduction in concrete used in their construction [2]. These higher strengths can be attributed to the confinement effect which is a result of the different elastic moduli of steel

Abbreviations: CFDST, concrete-filled double skin steel tubular (column); CFST, concrete-filled steel tubular (column); CHS, circular hollow section; SHS, square hollow section

* Corresponding authors.
E-mail addresses: mostafa.fahmi@f-eng.tanta.edu.eg (M.F. Hassanein), mohamed.elchalakani@uwa.edu.au (M. Elchalakani), yang0206@cqu.edu.cn (B. Yang).

https://doi.org/10.1016/j.istruc.2018.04.006
Received 7 December 2017; Received in revised form 2 April 2018; Accepted 18 April 2018
Available online 24 April 2018

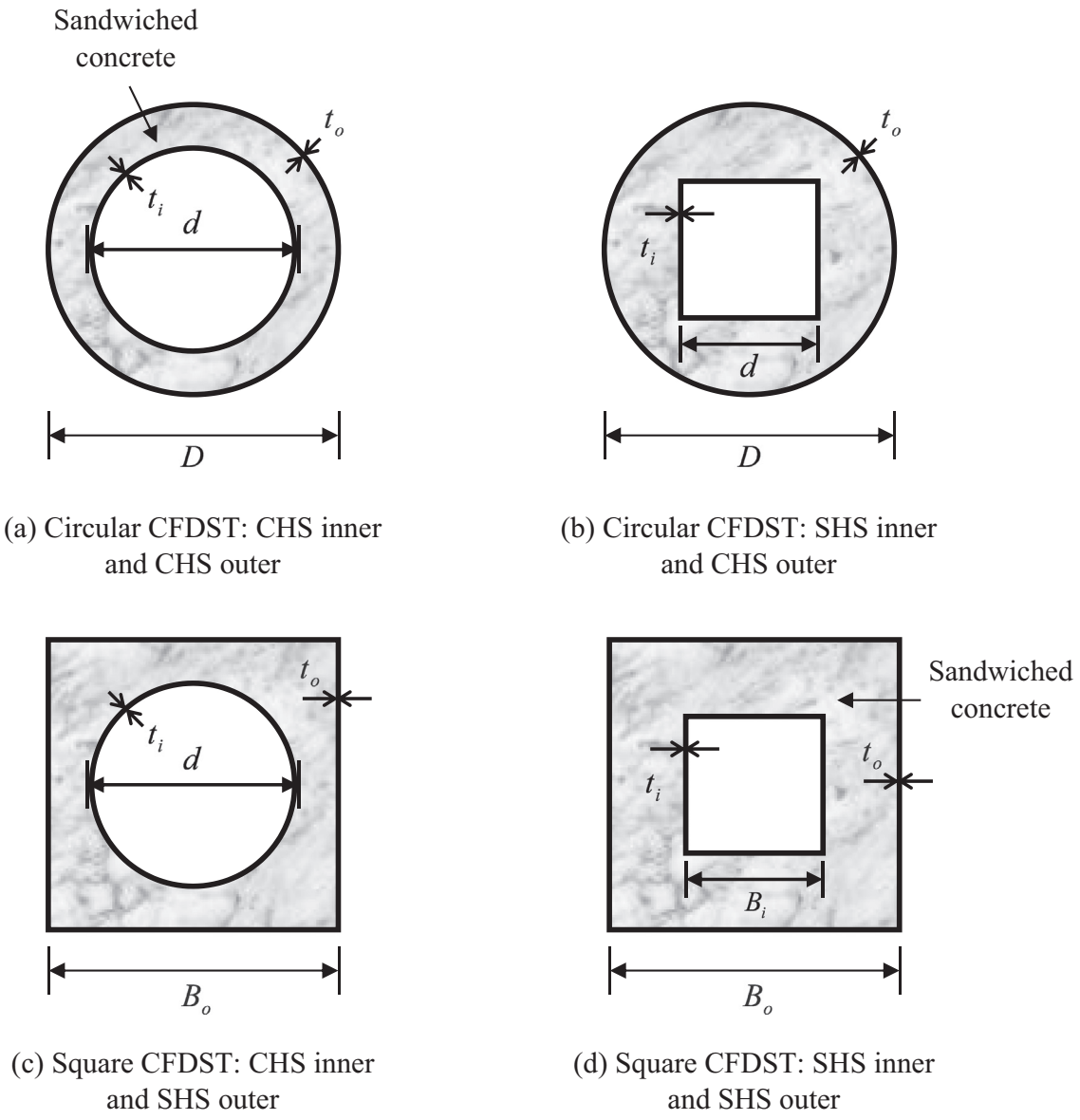

Fig. 1. Cross-section types of CFDST columns.

and concrete. Under compressive loading, the concrete in the column is more inclined to expand laterally than the two steel tubes. The steel, having a significantly higher stiffness, prevents this expansion and exerts lateral passive pressure back to the concrete [2]. The concrete in the CFDST columns experiences confinement from both inner and outer steel tubes, resulting in a “double-confinement effect” as opposed to the CFST columns which only produce a “single-confinement effect”. Recently, CFDST columns with different configurations have been under consideration in many experimental and numerical investigations; refer for example to Refs. [3–12]. However, most of these numerical investigations have used the constitutive material models of the steel and concrete originally suiting their behaviour in CFST columns with hot-rolled steel sections.

Despite the significant research conducted on CFDST columns with circular cross-sections [13], there is only a limited knowledge base on the behaviour of CFDST columns with SHS outer and SHS inner steel tubes [3,11]. Accordingly, this paper focuses on expanding this existing level of knowledge by investigating the behaviour of CFDST columns with SHS outer and SHS inner tubes (Fig. 1(d)) by considering the finite element (FE) program ABAQUS [14]. It is worth pointing out that this paper, rather than different investigations in literature, uses the most accurate constitutive model for the cold-formed steel (i.e. Ramberg-Osgood model) as used successfully by Elchalakani, et al. [2]. Furthermore, the appropriate confined concrete model for that filled in double-skin tubes is used as suggested by Zhao, et al. [11] and Pagoulatou, et al. [15], and the model providing the best validation is then considered. Six parameters are independently varied among the virtual test specimens. The effects of the slenderness ratio of the outer tube, the slenderness ratio of the inner tube, the hollow section ratio of the column, the compressive strength of the concrete used in the column and the yield strength of the steel tubes is examined. The scope of these tests however, exceeds the range of materials currently available in a laboratory. This program will be used to accurately predict the behaviour of CFDST columns under compressive loading when the aforementioned parameters are systematically changed. Then, the case of eccentric loading, which is rarely found in literature for the current cross-section, is examined.

2. Finite element methodology and validation

To simulate the behaviour of CFDST columns with SHS outer and SHS inner steel tubes, the FE program ABAQUS [14] was used. Once ABAQUS [14] is shown to produce accurate and reliable results, based on previous experimental data [3], the behaviour of the FE models generated in the parametric studies is predicted. Accordingly, in this section, the description of the FE modelling methodology used in the current investigation is given. Generally, the current FE models are based on that model described by Han, et al. [16], with some modifications as given in the next sections.

2.1. Elements and mesh utilised

The thin-walled steel tubes in CFST columns are generally discretized by shell elements (S4R) to capture the outwards local buckling modes induced from the lateral expansion of infilled concrete. However, it is noted that the size of shell element is larger than that of the tube thickness. This affects the discretisation of curved surfaces near the corners, especially the interaction between the concrete core and the steel tube. On the other hand, solid element (C3D8R) captures both the effective mesh at contact surfaces and the deflected shape of steel tubes [17–19]. Herein, each of the three parts forming the current CFDST short columns (outer steel tube, inner steel tube and concrete) was produced using a solid element. In particular, the eight-node elements endowed with reduced integration (C3D8R) as suggested by Elchalakani, et al. [2] was considered. However, in the current investigation, preliminary models were run using a shell element for the steel tubes in order to reduce computation time. The results coming from the preliminary models were not effectively found to reduce the solution time and, hence, the solid extrusion method was adopted. Fig. 2 shows the three-dimensional FE model of a typical CFDST column, from which an approximate global mesh size of the steel tubes and concrete infill was 10 and 9 mm, respectively.

2.2. Step type

Preliminary models were generated by used a static, general step. This, however, failed to produce accurate results compared with the test specimens [3]. This is attributed to the fact that this step type had difficulty converging due to contact or material complexities, which results in a large number of iterations. Instead, the compression step used throughout each of the ABAQUS models was a dynamic, explicit step. By using this step, the computation time obviously less than that of the static, general step, as the new system of equations is solved without iteration and the update of the system matrices is executed at the end of each time step. The inputs for this step were introduced under the mass scaling tab. This scaling took place throughout the whole model from the beginning of the step with a factor of 10. There was no target time increment. It is worth noting that for compatibility with the dynamic, explicit step only half of the cross-section of each column was used (see Fig. 2).

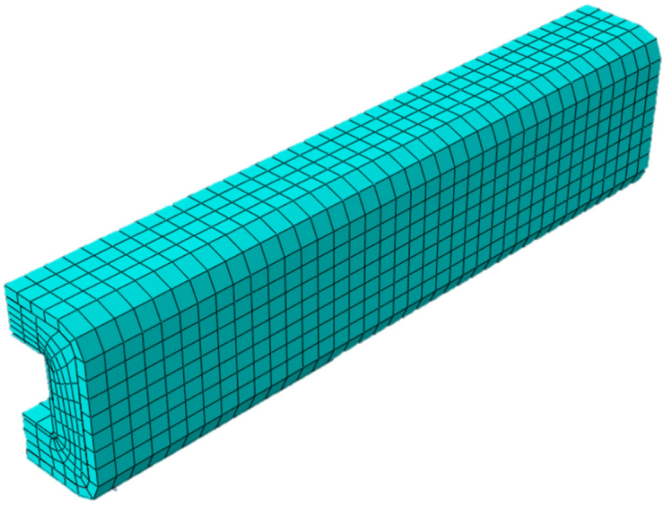

Fig. 2. Meshing methodology for a typical CFDST column.

2.3. Interactions

The interactions used in the ABAQUS models were surface-to-surface interactions. Each model required two interactions. The first was between the outer tube and the concrete section where the inner faces of the outer tube were the master surface and the outer faces of the concrete became the slave surface. Similarly, the second interaction occurs between the inner concrete faces (master surface) and the outer faces of the inner tube (slave surface). In the normal direction, the contact pressure-overclosure model was used, and the “normal behaviour” was selected as a “hard contact”. In the directions tangential to the surface, the Coulomb friction model was considered. More information on the effect of the friction in axially loaded stub tubed columns is presented by Liu, et al. [20].

The interaction component of the model was also used to create reference points at each end of the column. The first reference point (RP1) was located at the centre of the cross-section at the end of the column opposite the origin; see Fig. 3. The second reference point was therefore positioned at the origin. Both points were set as MPC constraints with the cross-section of the steel tubes and concrete section becoming the slave nodes.

2.4. Boundary conditions

Fig. 3 shows the boundary conditions used in the current FE models. As can be seen, a total of four boundary conditions were used for each ABAQUS model. The first condition fixed RP2 at the origin using the displacement/rotation type. Conversely, the second boundary condition was used to enable movement of RP1, also using the displacement/rotation type. Compression of the column was introduced through the third boundary condition which set the value of U3 to −20. Finally, the fourth boundary condition was used to complete the symmetry of the column in the direction of the x-axis. It is worth noting that the above described loading ensures that the load is evenly distributed over the upper cross-section of the axially loaded composite column; for other loading conditions, the paper by Zhou, et al. [21] worth to be read.

2.5. Stress-strain relationship for structural steel

The stress-strain relationship for the precise simulation of cold-formed steel tubes was obtained by using the Ramberg-Osgood model as suggested by Elchalakani, et al. [2]. The Ramberg-Osgood model consists of the creation of the engineering stress-strain curve, which is then corrected to the true stress-strain curve as shown in Fig. 4. The

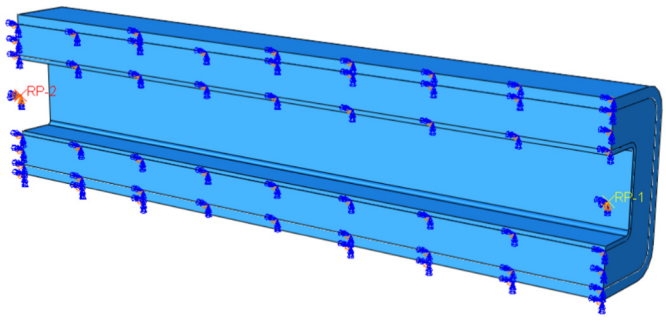

Fig. 3. Boundary conditions and RPs for a typical CFDST column.

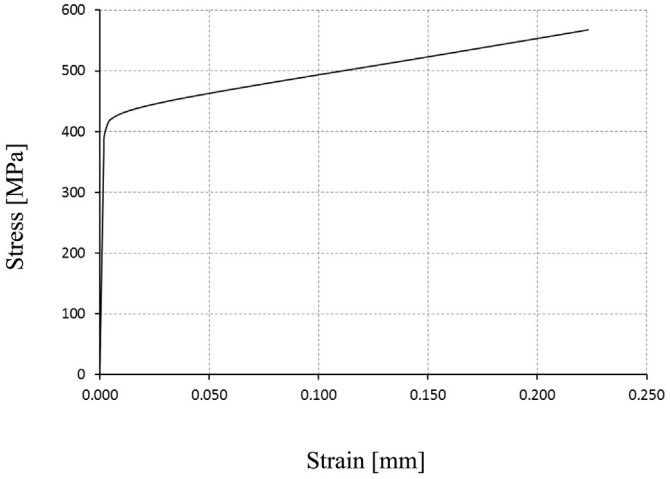

Fig. 4. Typical Ramberg-Osgood stress-strain curves [2].

Ramberg-Osgood coefficient (n) was calculated based on MMPDS-01, and it is obtained by the following equation:

$$\varepsilon = \frac{\sigma}{E} + 0.002\left(\frac{\sigma}{F_{ty}}\right) \tag{3}$$

In the FE analysis, the steel material is considered as an elastic material until its yield stress. After that point, it is simulated as a plastic material. The modulus of elasticity (E_s) was assumed equal to 203GPa as recommended by the AISC 360-10 [22] and the Poisson's ratio (ν) was taken as 0.3.

2.6. Constitutive model of the sandwiched concrete

Two models were checked in the concrete validation process in order to reach the most accurate constitutive model for the sandwiched concrete. The first is the Mander model modified for the double SHS geometry as suggested by Zhao, et al. [11], termed hereafter as Zhao model. For the sake of consistency with colleagues investigating CFDST columns with CHS geometries, the second concrete model used by Pagoulatou, et al. [15], given after this as the Pagoulatou model, was as well considered in this validation process. The load-axial deflection curves produced by ABAQUS [14], by using both concrete models given above, were compared with the experimental specimens tested by Zhao and Grzebieta [3]. It is worth noting that the concrete material is treated as plastic with the Drucker-Prager option [23]. Hence, the angle of friction and the flow stress ratio can be set to 20° and 0.8, respectively [15].

2.6.1. Zhao model

The concrete model proposed by Zhao, et al. [11], consists of the following series of equations:

$$\sigma_{concrete} = \frac{f_{cc}\left(\frac{\varepsilon}{\varepsilon_{cc}}\right) r_m}{r_m - 1 + \left(\frac{\varepsilon}{\varepsilon_{cc}}\right)^{r_m}} \tag{4}$$

$$f_{cc} = f_c\left[1 + \left(\frac{t_o}{B_o}\right)\left(\frac{f_{yo}}{f_c}\right)\right] \tag{5}$$

$$\varepsilon_{cc} = \varepsilon_{co}\left[1 + 5\left(\frac{f_{cc}}{f_c} - 1\right)\right] \tag{6}$$

$$\varepsilon_{co} = 0.002 + 0.001\left(\frac{f_c - 20}{80}\right) \tag{7}$$

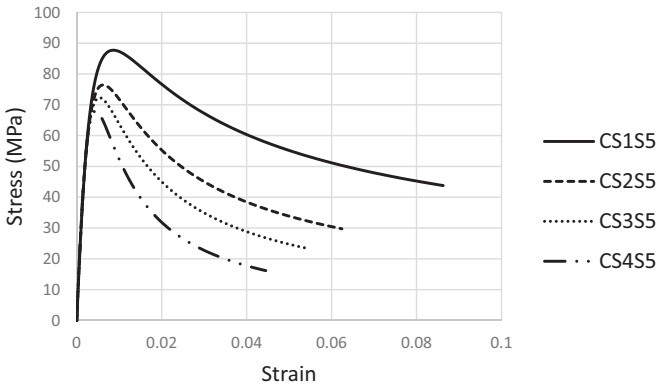

Fig. 5. Zhao concrete model [11] stress-strain curves of experimental specimens [3].

$$r_m = \frac{E_c}{E_c - E_{sec}} \tag{8}$$

$$E_c = 3320\sqrt{f_c} + 6900 \tag{9}$$

$$E_{sec} = \frac{f_{cc}}{\varepsilon_{cc}} \tag{10}$$

This model is represented graphically in Fig. 5 for the 4 pairs of experimental specimens tested by Zhao and Grzebieta [3].

2.6.2. Pagoulatou model

The concrete model proposed by Pagoulatou, et al. [15], as shown in Fig. 6, consists of the following series of equations [24,25]:

$$f_{cc} = f_c + k_1 f_1 \quad \text{where } k_1 = 4.1 \tag{11}$$

$$\varepsilon_{cc} = \varepsilon_c\left(1 + k_2\frac{f_1}{f_c}\right) \quad \text{where } k_2 = 20.5 \tag{12}$$

$$f_1 = 8.525 - 0.166\left(\frac{B_o}{t_o}\right) - 0.00897\left(\frac{B_i}{t_i}\right) + 0.00125\left(\frac{B_o}{t_o}\right)^2 + 0.00246\left(\frac{B_o}{t_o}\right)\left(\frac{B_i}{t_i}\right) - 0.0055\left(\frac{B_i}{t_i}\right)^2 \geq 0 \tag{13}$$

$$\frac{f_1}{f_{yi}} = 0.01844 - 0.00055\left(\frac{B_o}{t_o}\right) + 0.0004\left(\frac{B_i}{t_i}\right) + 0.00001\left(\frac{B_o}{t_o}\right)^2 + 0.00001\left(\frac{B_o}{t_o}\right)\left(\frac{B_i}{t_i}\right) - 0.00002\left(\frac{B_i}{t_i}\right)^2 \tag{14}$$

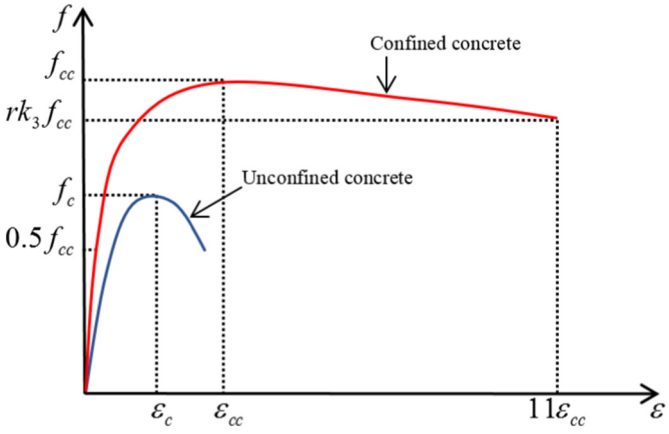

Fig. 6. Stress-strain curves for concrete Pagoulatou, et al. [15].

$$\frac{f_l}{f_{yo}} = 0.01791 - 0.00036\left(\frac{B_o}{t_o}\right) - 0.00013\left(\frac{B_i}{t_i}\right) + 0.00001\left(\frac{B_o}{t_o}\right)^2 + 0.00001\left(\frac{B_o}{t_o}\right)\left(\frac{B_i}{t_i}\right) - 0.00002\left(\frac{B_i}{t_i}\right)^2 \quad (15)$$

$$\sigma_{concrete} = \frac{E_c\varepsilon}{1 + (R + R_E - 2)\left(\frac{\varepsilon}{\varepsilon_{cc}}\right) - (2R - 1)\left(\frac{\varepsilon}{\varepsilon_{cc}}\right)^2 + R\left(\frac{\varepsilon}{\varepsilon_{cc}}\right)^3} \quad (16)$$

$$E_c = 4700\sqrt{f_{cc}} \quad (17)$$

$$R = \frac{R_E(R_\sigma - 1)}{(R_\varepsilon - 1)^2} - \frac{1}{R_\varepsilon}$$
where $R_\sigma = 4$ and $R_\varepsilon = 4$ (Hu & Schnobrich) (18)

$$R_E = \frac{E_c\varepsilon_{cc}}{f_{cc}} \quad (19)$$

In this model, the last point on the concrete stress-strain curve is estimated at a stress given by the expression rk_3f_{cc}, which occurs at a strain value of $11\varepsilon_{cc}$. In this expression, r is a reduction factor taken as 1.0 for concrete strengths of 30 MPa and below and 0.5 for concrete strengths of 100 MPa and above. A linear interpolation is used for concrete strengths between 30 MPa and 100 MPa. The parameter k_3 is given by the expression below:

$$k_3 = 1.73916 - 0.00862\left(\frac{B_o}{t_o}\right) - 0.04731\left(\frac{B_i}{t_i}\right) + 0.00036\left(\frac{B_o}{t_o}\right)^2 + 0.00134\left(\frac{B_o}{t_o}\right)\left(\frac{B_i}{t_i}\right) - 0.00058\left(\frac{B_i}{t_i}\right)^2 \geq 0 \quad (20)$$

To account for the effects of the column size, the concrete quality and the loading rate on the unconfined concrete compressive strength (f_c), a slight modification for both models [11,15] has been undertaken herein similar to that considered by the authors in Ref. [12] which investigated the square CFDST columns with inner circular tubes. According to this modification, the unconfined concrete compressive strength has been reduced to the value $\gamma_c f_c$. γ_c is the strength reduction factor suggested by Liang [26], which is a function of the depth of the concrete core (D_c) as follows:

$$\gamma_c = 1.85D_c^{-0.135} \quad (0.85 \leq \gamma_c \leq 1.0) \quad (21)$$

2.7. Validation of the FE model

Validation of the current models involved comparison of previous experimental specimens of Zhao and Grzebieta [3] with the corresponding ABAQUS model considering both concrete models given above. Zhao and Grzebieta [3] tested eight specimens, from which each two are replicates to ensure the accuracy of the test procedure. Herein, comparisons between the experimental and the FE modelling are made by considering the ultimate loads, the load-axial displacement curve and the observed failure mechanism. Table 1 provides the comparison between the experimental ultimate loads ($P_{ul,Exp}$) and the FE models considering the concrete models of Zhao model [11] ($P_{ul,FE,Z}$) and Pagoulatou model [15] ($P_{ul,FE,P}$). However, this table shows that both constitutive models of concrete capture the ultimate load of the CFDST columns properly. On the other hand, Fig. 7 shows the load-axial deflection relationships for the columns considering the experimental and FE responses. To the left of the figure, the comparison is made between the experiments and those models considering Zhao's concrete constitutive model [11], while to comparison with the Pagoulatou model [15] is shown to the right. Overall, both concrete constitutive models [11,15] give accurately the experimental recorded load-axial deflection relationships. For all the specimens, using both concrete constitutive models [11,15] provides the typical experimental behaviour of the CFDST columns until the ultimate load is reached, while the post-ultimate load stage is not presented well by the Pagoulatou's concrete model [15] for columns CS3S5 and CS4S5 whom are characterised by their high plate slenderness ratios ($B_O/t_o \geq 33$). As can be noticed, this model [15] shows higher post-ultimate load stage compared with the experiments. This could be attributed to the difference in post-peak portion of the stress-strain models; while it is curved (with a concave shape) in the Zhao model [11] it is a straight line in that of Pagoulatou model [15]. Hence, Zhao model [11] fits the experimental results more accurately. Despite the insignificance of the post-ultimate stage in design, the Zhao model [11] was selected for the parametric studies based on its accuracy along all behavioural loading stages. To further trust this selected model, Figs. 8–11 display the failure modes of both the outer and inner steel tubes observed from the ABAQUS models. The outer tube deformation shape was consistent across each of the four specimens tested, showing all faces of the tube bulging outwards as seen in the corresponding experimental tests. On the other hand, the inner tube exhibited two main deformations pattern. There was negligible change to the inner tube in specimens CS1S5 (Fig. 8) and CS2S5 (Fig. 9), while specimens with CS3S5 (Fig. 10) and CS4S5 (Fig. 11) buckled in the same fashion as their experimental counterparts; see the circles added to these figures. Based on these comparisons, the concrete model proposed by Zhao, et al. [11], produced accurate and reliable results.

3. Parametric studies

A total of twenty CFDST columns were analysed to consider the effects of the dimensions and material properties of the square CFDST short column with inner SHSs. These were divided into five groups of four specimens within each group independently investigating the effect of a given parameter. In these parametric studies, the steel and concrete materials have values ranging from normal to very high strength [27,28]. The very high strength steel is supported by the recent availability of such steels in Australia [27], while the very high strength concrete is available globally [28]. It is worth pointing out that the values of both the f_c and f_y should be compatible. This has, however,

Table 1
Nominal dimensions of the test specimens [3] and comparisons between the experimental and FE ultimate loads.

Specimen	B_o [mm]	t_o [mm]	B_i [mm]	t_i [mm]	$P_{ul,FE,Z}$ [kN]	$P_{ul,FE,Z}$ [kN]	$P_{ul,FE,P}$ [kN]	$\frac{P_{ul.FE,Z}}{P_{ul,Exp}}$	$\frac{P_{ul.FE,P}}{P_{ul,Exp}}$
CS1S5A	100	6.0	50	2.0	1545	1522	1578	0.99	1.02
CS1S5B		6.0			1614	1522	1578	0.94	0.98
CS2S5A		4.0			1194	1189	1197	1.00	1.00
CS2S5B		4.0			1210	1189	1197	0.98	0.99
CS3S5A		3.0			1027	1037	1042	1.01	1.01
CS3S5B		3.0			1060	1037	1042	0.98	0.98
CS4S5A		2.0			820	824	830	1.00	1.01
CS4S5B		2.0			839	824	830	0.98	0.99
Average								0.99	1.00
Standard deviation								0.021	0.016

Zhao model [11] Pagoulatou model [15]

(1) CS1S5

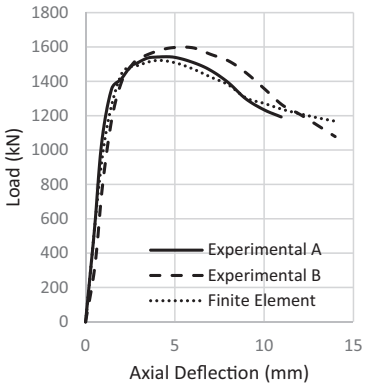

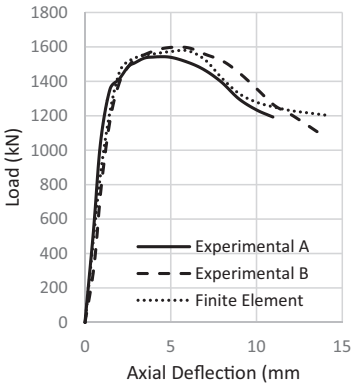

(2) CS2S5

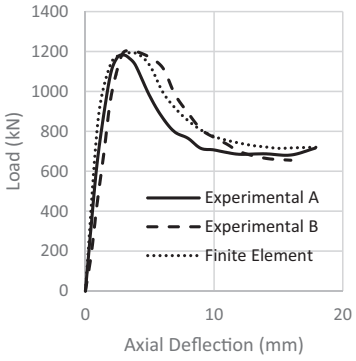

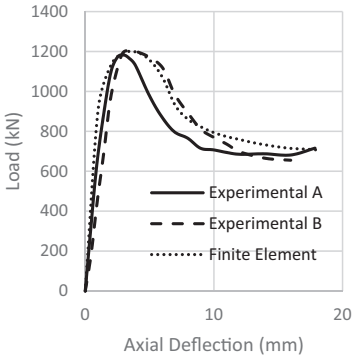

(3) CS3S5

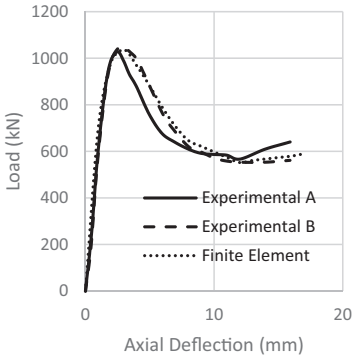

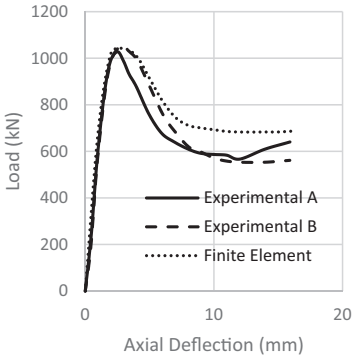

(4) CS4S5

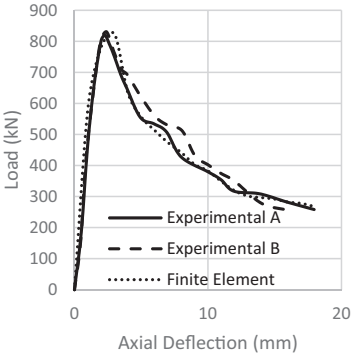

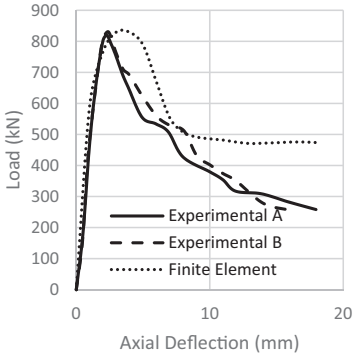

(caption on next page)

Fig. 7. Comparisons between experimental and FE load-axial deflection relationships.

been insured following the recommendation on the matching grades of steel and concrete suitable for use in CFST columns given by Liew, et al. [28]. From this analysis, load-axial deflection curves were obtained and strength-to-weight ratios were calculated for each column. In addition to this, a series of moment-interaction diagrams was also produced for each group of specimens under the effect of eccentric compression. Table 2 provides the details of these parametric studies considered.

3.1. Group 1: effects of the outer tube thickness

The first group of specimens generated, investigates the impact of reducing the thickness of the outer steel tube on the overall compressive behaviour of the column. The thickness was reduced to create outer steel tubes with slenderness ratios ranging from 51.6 (specimen OT1) to 292.2 (specimen OT4). The results of this group of testing are presented in Fig. 12 and Table 3.

Fig. 12 shows a significant reduction in the capacity of the columns as the slenderness ratio of the outer tube is increased (i.e. the thickness of the outer tube is reduced). This is a logical outcome which can be attributed to the reduction in concrete confinement as the outer tube slenderness ratio increases. As the thickness of the outer tube is reduced, there is a greater axial deflection in the tube prior to failure. The greater the deflection of the steel tube is, the greater the reduction in compressive mean strain of the concrete is, which in turn decreases the effect of confinement in the concrete section. However, the stiffness of the curves shows insignificant increase as the tube thickness increases,

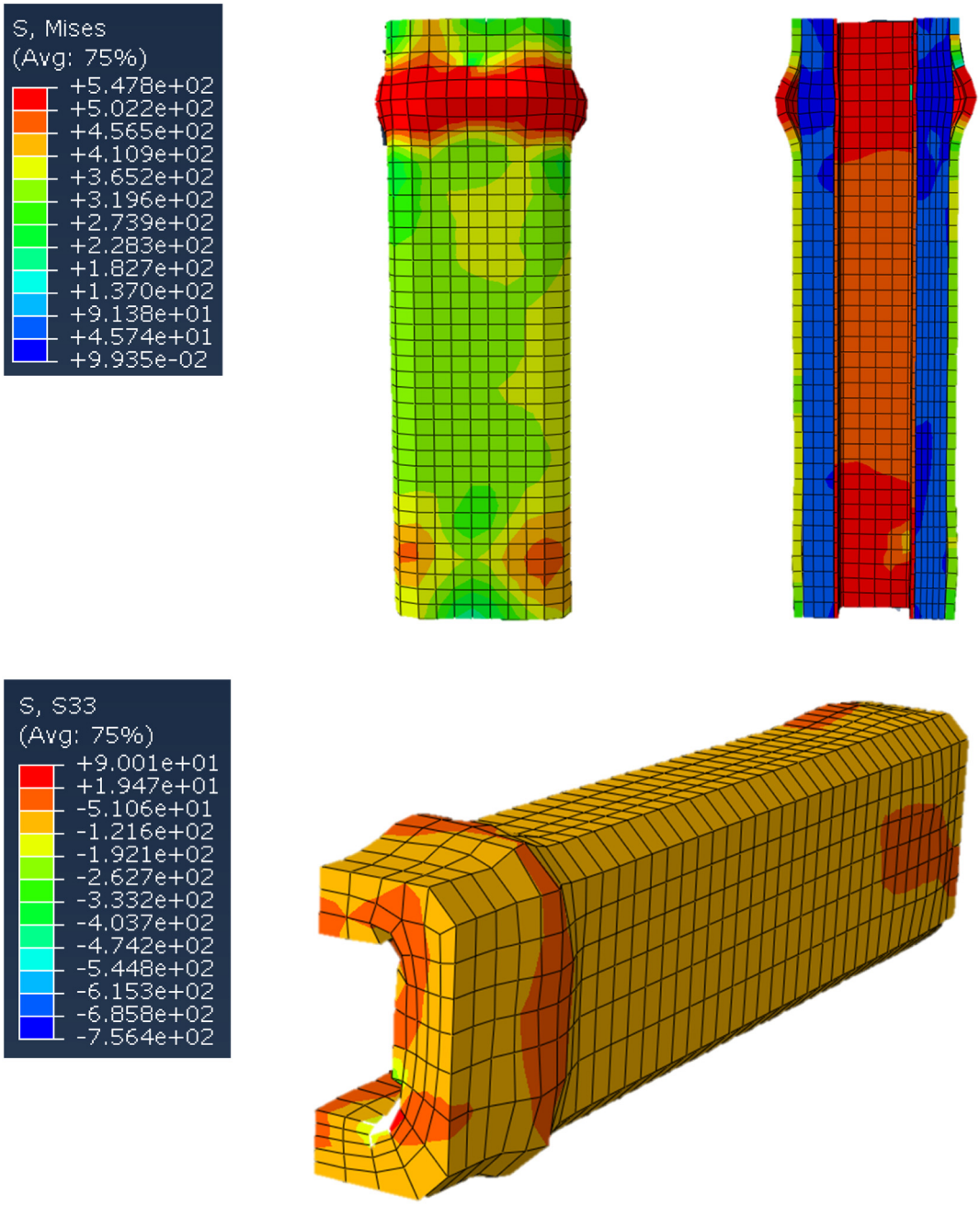

Fig. 8. FE Final deformation shapes of specimen CS1S5 - typical to experiment CS1S5B.

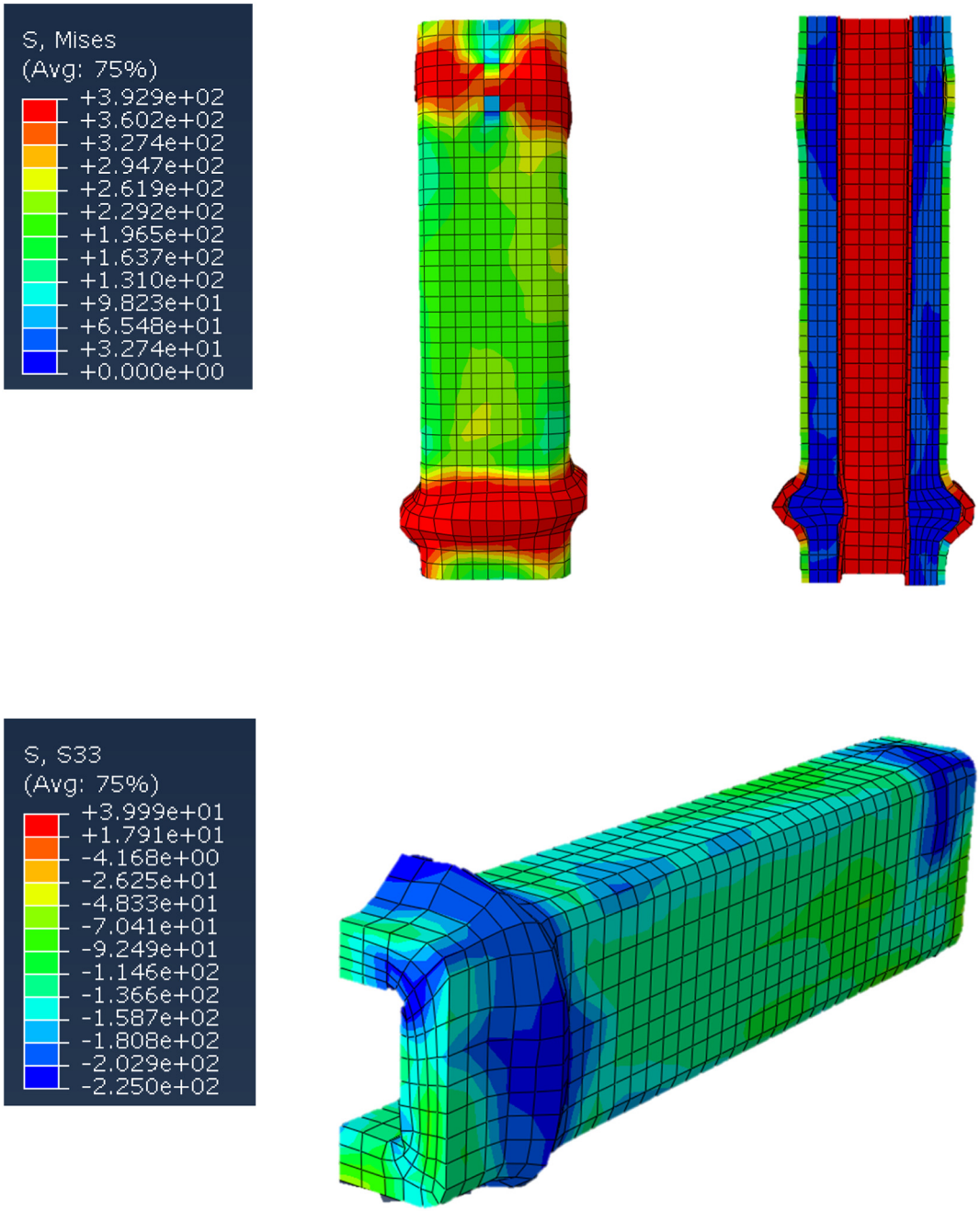

Fig. 9. FE Final deformation shapes of specimen CS2S5 - typical to experiment CS2S5A.

and the residual strength part remaining after the ultimate load seems parallel to each other.

As this outer tube thickness decreases however, so does the weight of the column; given less steel is being used. Table 3 presents this reduction in the weight of the column across the four specimens as well as the corresponding strength-to-weight ratios. It shows that as the thickness of the outer tube is reduced, the strength-to-weight ratio of the column also decreases. This indicates that the decline in the capacity of the column outweighs the reduction in its weight. For a study in optimising the strength-to-weight ratio of the column, Table 3 confirms that reducing the thickness of the outer tube is an inefficient method. The reduction in column capacity is too significant for the benefit of the weight reduction to overcome and as a result, the strength-to-weight ratio of the column declines as the slenderness ratio of the outer steel tube increases.

3.2. Group 2: effects of the inner tube thickness

The second test group investigates the effect of reducing the thickness of the inner steel tube. Across the four specimens tested, the inner tube thickness was reduced to produce tubes with slenderness ratios ranging from 50.3 (specimen IT1) to 208.2 (specimen IT4), from which the results of this test group are displayed in Fig. 13 and Table 4.

Fig. 13 and Table 4 illustrate a minor reduction in column capacity as the thickness of the inner tube is reduced. Again, this is to be expected, given the inner tube contributes to the confinement of the concrete, albeit to a lesser extent than the outer tube. As the thickness of the inner tube is reduced, it experiences more significant lateral deflection prior to failure. The greater this deflection is, the lower the compressive strain in the concrete and the lower the concrete confinement is. This effect is less notable than what was observed with the Group 1 specimens because the outer tube contributes more

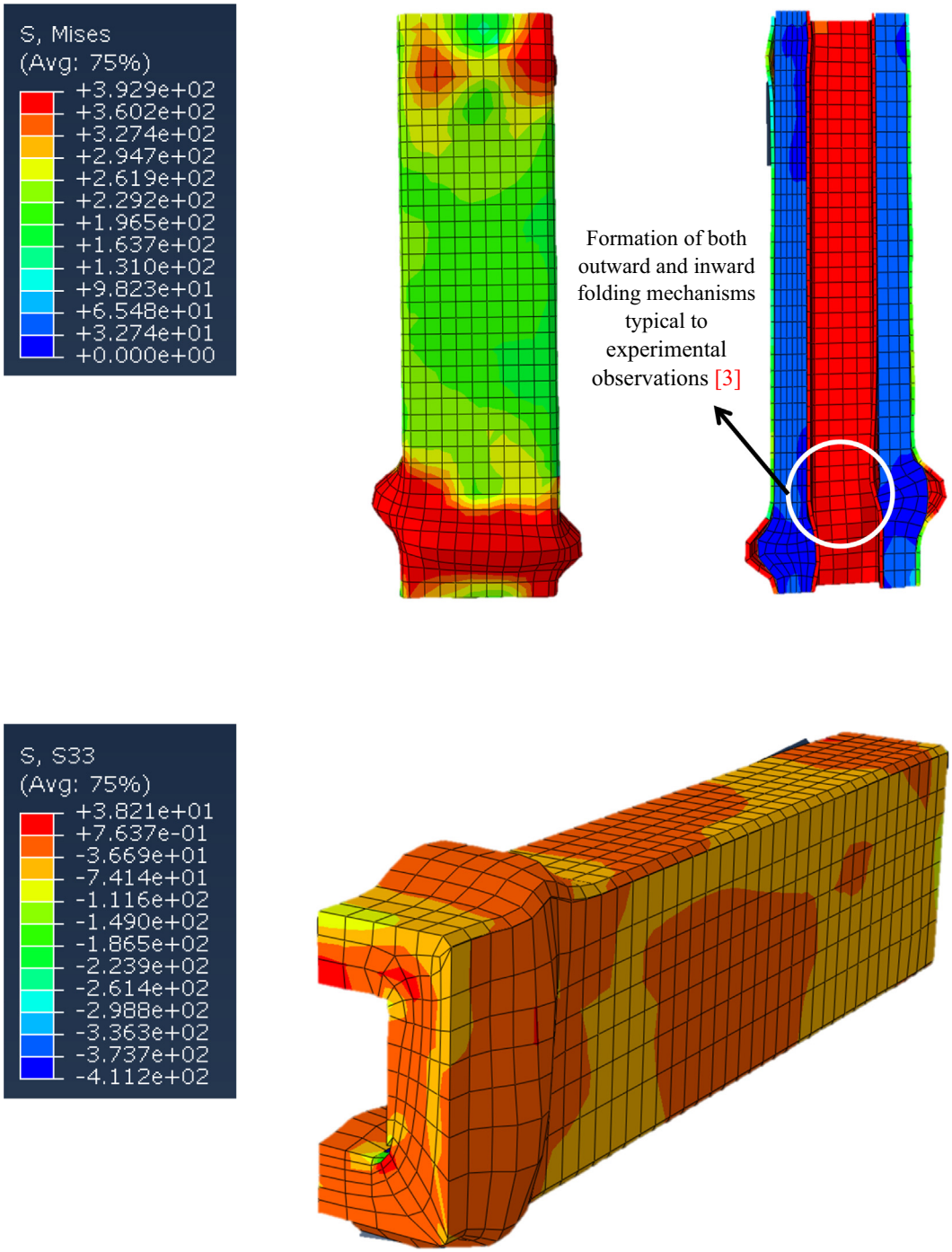

Fig. 10. Final deformation shapes of specimen CS3S5 - typical to experiment CS3S5B.

prominently to the amount of steel in the column and hence, the overall confinement of the concrete. The trend in the two groups of models however, is the same; increasing the slenderness ratio of the inner steel tube reduces the overall capacity of column. Nevertheless, the Load-axial deflection curves are almost the same for all the columns with different inner tube thickness in terms of the initial stiffness and the residual strength after ultimate load.

The reduction in inner tube thickness also brings about a decline in the weight of the column. However, Table 4 shows that despite this improvement in the weight of the column, the strength-to-weight ratio of the columns steadily decreases as the inner tube thickness is reduced. While the magnitude of this decline is not as considerable as that observed for Group 1 specimens, the trend remains that the reduction in the weight of the column is not worth the cost of overall capacity. As was observed with the outer tube, increasing the slenderness ratio of the inner steel tube is not an effective way to improve the strength-to-weight ratio of the column. Hence, the inner tube thickness might be taken as least as possible in order to reduce the cost of the column in practice.

3.3. Group 3: effects of hollow section ratio

The four specimens tested in Group 3 were used to investigate the effect of the hollow section ratio (χ) of the column. This was tested by increasing the width of the inner steel tube across the four specimens while the other dimensions remained constant. The hollow section ratio

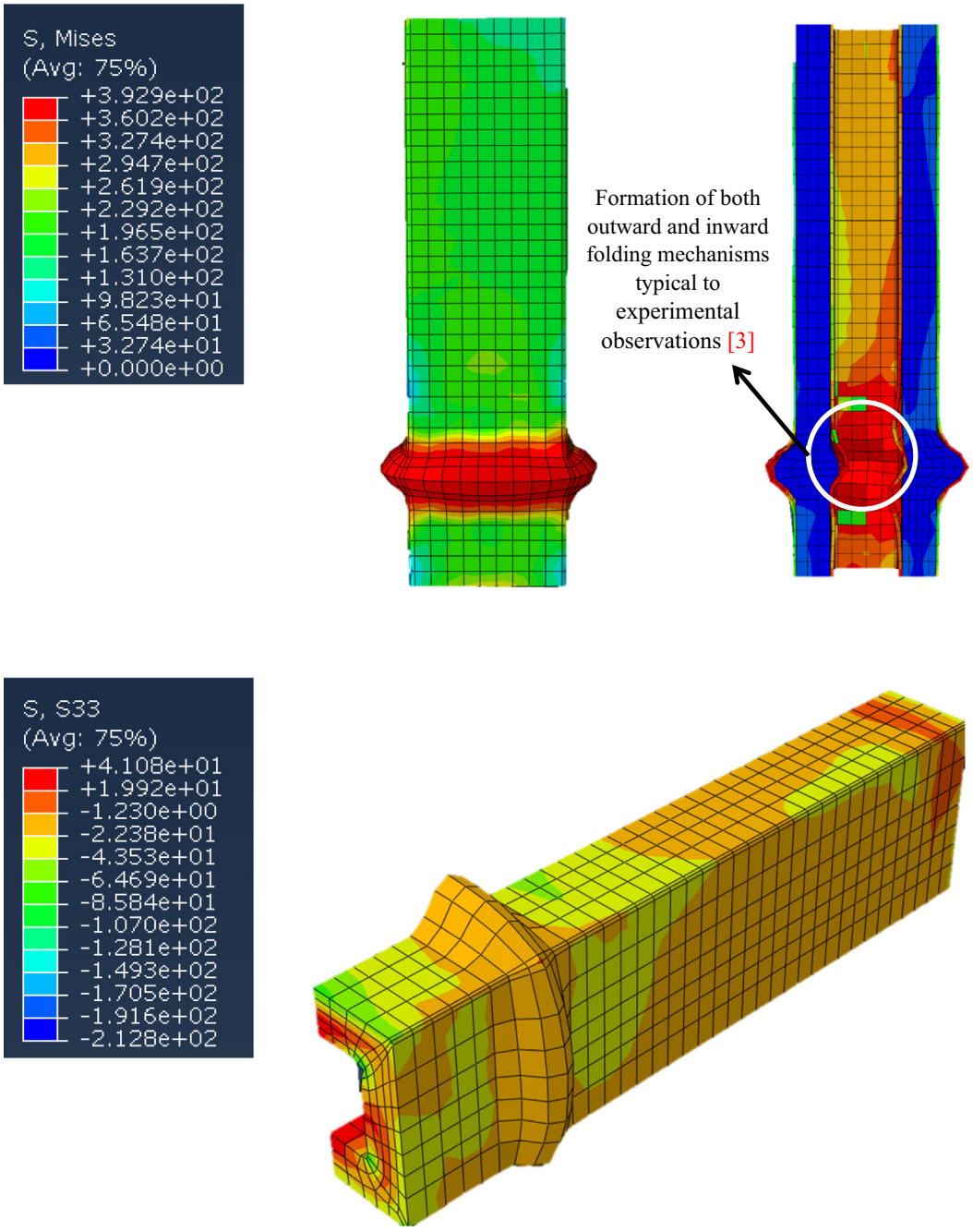

Fig. 11. FE Final deformation shapes of specimen CFS4S5 - typical to experiment CS4S5A.

was varied from 0.1 (specimen HR1) to 0.6 (specimen HR4). The results of these tests are shown in Fig. 14 in terms of the load axial-deflection curves and in Table 5 as the Strength-to-Weight ratios. Fig. 14 shows a positive correlation between the hollow ratio and ultimate capacity of the square CFDST columns with inner SHSs. As the hollow ratio is increased, the behaviour of the column shifts from that of a traditional CFST column, to a more conventional CFDST column. The significance of the hollow ratio is the position of the maximum concrete stress. As the hollow section ratio increases, this maximum stress moves from the inner steel tube to the centre of the concrete section which in turn improves the overall capacity of the column. An additional benefit of the increased hollow section ratio is the reduced weight of the column given the volume of concrete removed from the central core of the column. It is clear that increasing the width of the inner steel tube results in less concrete in the column, which significantly reduces the weight of the column. This besides shifting the position of the maximum concrete stress to the concrete section has a two-fold effect on the strength-to-weight ratio of the column. While the initial stiffness remains the same, it is worth pointing out that increasing the χ ratio provides higher residual resistance after failure, which would be of importance in cases of overloading collapse.

As shown in Table 5, increasing the hollow section ratio of the column from specimen HR1 to HR4 increases the capacity of the column, while reducing its overall weight. Across the four specimens, the strength-to-weight ratio is improved by almost 12% as the hollow ratio is varied from 0.1 to 0.6. This indicates that altering the hollow ratio of CFDST columns is an effective way of improving the capacity of the column as well as the strength-to-weight ratio, which is opposite to the effects of the previous two key factors.

Table 2
Details of the generated parametric studies.

Group	Specimen	Outer tube			Inner tube			L [mm]	χ	f_c [MPa]	f_y [MPa]	Ecc. [mm]
		B_o [mm]	t_o [mm]	λ	B_i [mm]	t_i [mm]	λ					
1 (OT)	OT1	219.1	4.8	51.64	89	6.0	15.18	700	0.42	60	350	–
	OT2		3.0	84.05					0.42			
	OT3		2.0	127.3					0.41			
	OT4		0.88	292.2					0.41			
2 (IT)	IT1	219.1	8.2	29.25	89	2.0	50.29	700	0.44	60	350	–
	IT2					1.5	67.84					
	IT3					1.0	102.9					
	IT4					0.5	208.2					
3 (HR)	HR1	219.1	8.2	29.25	21	2.0	10.06	700	0.10	60	350	–
	HR2				55	4.0	13.90		0.27			
	HR3				88	7.0	12.51		0.43			
	HR4				122	9.0	13.67		0.60			
4 (CS)	CS1	219.1	8.2	29.25	89	6.0	15.18	700	0.44	60	350	–
	CS2									100		
	CS3									140		
	CS4									180		
5 (SS)	SS1	219.1	8.2	29.25	89	6.0	15.18	700	0.44	60	350	–
	SS2			41.36			21.47				700	
	SS3			50.66			26.30				1050	
	SS4			58.50			30.37				1400	
6 (E)	E1	219.1	8.2	29.25	89	6.0	15.18	700	0.44	60	350	13.69
	E2											27.39
	E3											54.78
	E4											109.55

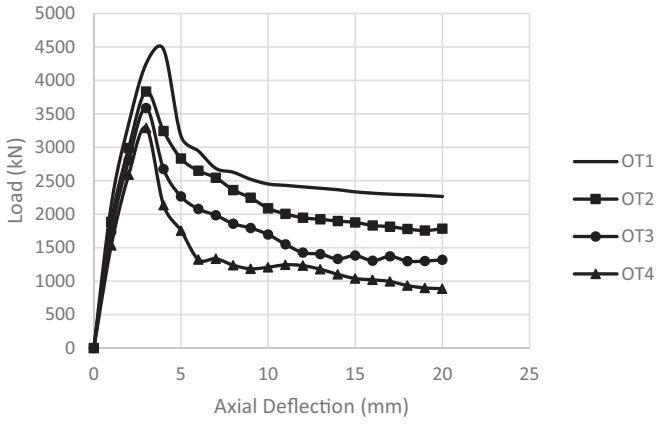

Fig. 12. Load-axial deflection curves for Group 1 specimens.

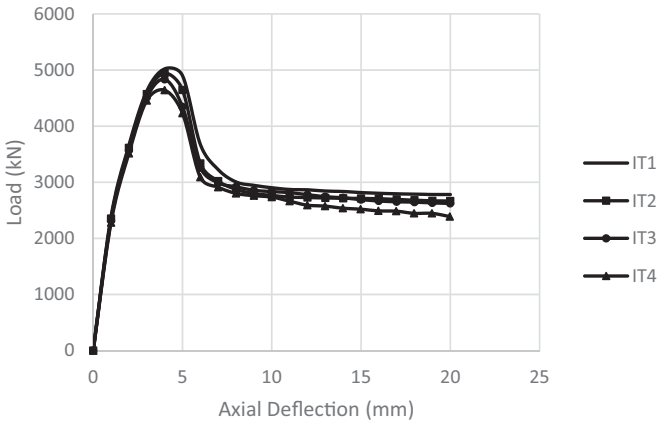

Fig. 13. Load-axial deflection curves for Group 2 specimens.

Table 3
Strength-to-weight ratios for Group 1 specimens.

Specimen	$P_{ul,FE}$ [kN]	Weight (kg)	Strength-to-weight ratio (kN/kg)
OT1	4464.6	91.1	49.0
OT2	3833.5	86.8	44.2
OT3	3587.6	84.3	42.6
OT4	3290.6	80.9	40.7

Table 4
Strength-to-weight ratios for Group 2 specimens.

Specimen	$P_{ul,FE}$ [kN]	Weight (kg)	Strength-to-weight ratio (kN/kg)
IT1	5021.2	91.1	55.1
IT2	4943.6	90.2	54.8
IT3	4834.0	89.3	54.1
IT4	4641.8	88.3	52.6

3.4. Group 4: effects of concrete compressive strength

Group 4 test specimens investigate the influence of the concrete strength on the general behaviour and the ultimate capacity of the current CFDST columns. The strength of the concrete used in the columns was increased from 60 MPa (specimen CS1) to 180 MPa (specimen CS4). The results of these tests are shown in Fig. 15 and Table 6.

The curves displayed in Fig. 15 present an obvious result; as the strength of the concrete is increased, so is the ultimate capacity of the column. The important outcome from this series of tests however, is the efficiency of this increase in concrete strength calculated in Table 6. When compared with specimen CS1 (concrete strength of 60 MPa), specimen CS2 produces a 23.8% increase in ultimate capacity despite the 66.7% increase in the strength of the concrete used in its construction. This trend is repeated in specimens CS3 (133.3% stronger concrete) and CS4 (200% stronger concrete), which exhibit ultimate capacity increases of only 49.2% and 67.3%. Moderating these figures reveals an average efficiency of 35.4% across the four specimens. Given the added expense incurred with increasing the strength of concrete, an efficiency of approximately 35% indicates this is not a worthwhile method of improving the overall capacity of CFDST columns.

Another trend that can be detected from the axial-load deflection

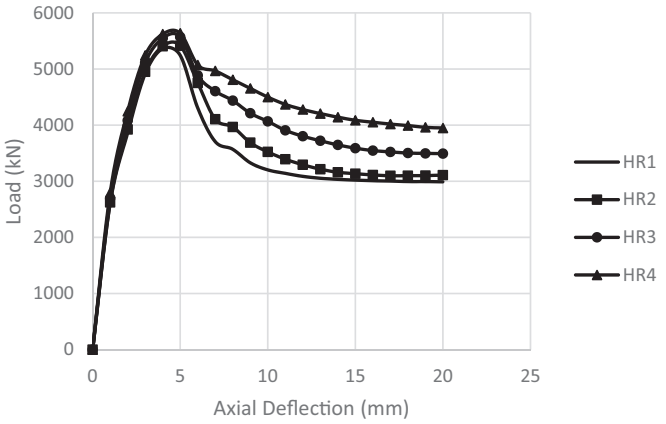

Fig. 14. Load axial-deflection curves for Group 3 specimens.

Table 5
Strength-to-weight ratios for Group 3 specimens.

Specimen	$P_{ul,FE}$ [kN]	Weight (kg)	Strength-to-weight ratio (kN/kg)
HR1	5364.7	100.9	53.2
HR2	5414.8	99.6	54.4
HR3	5571.3	98.3	56.7
HR4	5638.0	94.8	59.5

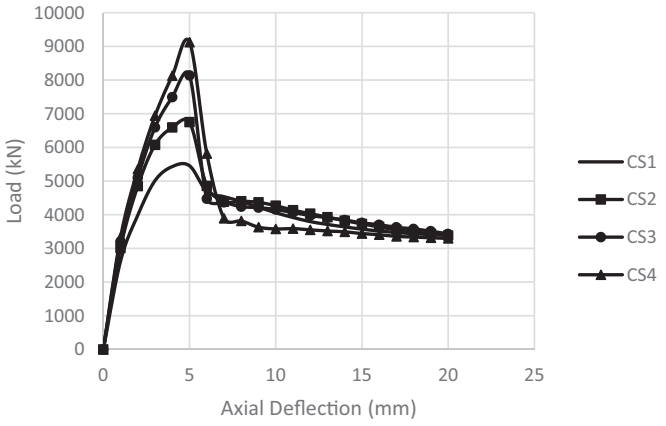

Fig. 15. Load-axial deflection curves for Group 4 specimens.

Table 6
Concrete strength efficiency for Group 4 specimens.

Specimen	Capacity (kN)	Increase in capacity (%) (1)	Increase in concrete strength (%) (2)	(1)/(2)
CS1	5453.7	–	–	–
CS2	6750.8	23.8	66.7	0.355
CS3	8139.4	49.2	133.3	0.369
CS4	9125.0	67.3	200.0	0.337

curve is the method of failure of the columns. As Fig. 15 shows, as the strength of the concrete is increased, so is the peak point on the curve. However, the post-peak behaviour of the curve shows a rapid decline in column capacity; suggesting brittle failure. From a construction perspective, this is a less than favourable result. This graph indicates that once the peak capacity of the column is reached, any additional loading applied to the column will bring about a very sudden failure with limited warning. Physically, this could result in the concrete cracking abruptly and potentially shattering, should the applied loads be great

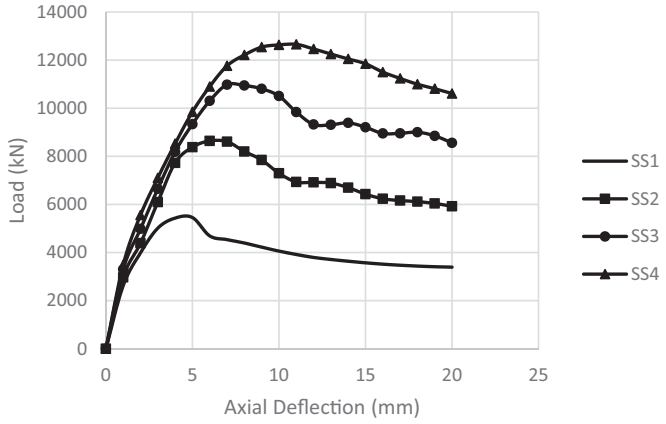

Fig. 16. Load-axial deflection curves for Group 5 specimens.

enough. Based on the curves in Fig. 15, this trend becomes increasingly prominent with stronger concrete and presents a possible field for future experimental investigation.

3.5. Group 5: effects of steel strength

The four specimens in Group 5 were used to test the effect of increasing the yield stress of the steel tubes used in the current CFDST columns with both SHSs. The steel strength was increased from 350 MPa (specimen SS1) to 1400 MPa (specimen SS4). The results of these tests are shown in Fig. 16 and Table 7.

The curves shown in Fig. 16 demonstrate a similar trend to that of the Group 4 specimens whereby an increase in steel strength significantly improves the capacity of the CFDST column. As shown in Table 7, however, this increase in capacity is relatively inefficient when compared to the corresponding increase in steel strength. Across specimens SS2, SS3 and SS4, the steel strength is increased from 700 MPa to 1400 MPa, nevertheless, this increase yields an increase in capacity of only 58.4%, 101.3% and 132.0%, respectively. Another important trend appears in the final column of Table 7. This represents the efficiency of the steel strength and shows that as the strength of the steel is increased, this efficiency declines from 58.4% to 44.0%. This suggests that although increasing the steel strength improves the capacity of the column, this is not a very efficient approach.

As with the specimens examined in Group 4, the curves in Fig. 16 can be used to indicate the expected failure modes of the columns. Each curve shown in Fig. 16 exhibits a similar shape which is characterised by a steady post-peak decline until the final load. Unlike the Group 4 specimens, this is an encouraging result. The smooth and steady post-peak behaviour of these columns implies a ductile failure mode where the columns fail slowly and provide sufficient warning that failure is about to occur. In a construction setting, this is obviously preferred than the failure mode of the Group 4 specimens which would be rapid and without warning. Importantly, the post-peak region of the axial-load deflection curve becomes smoother and steadier as the strength of the steel in increased.

Table 7
Steel strength efficiency for Group 5 specimens.

Specimen	Capacity (kN)	Increase in capacity (%) (1)	Increase in steel strength (%) (2)	(1)/(2)
SS1	5453.7	–	–	–
SS2	8639.7	58.4	100.0	0.584
SS3	10,977.6	101.3	200.0	0.507
SS4	12,655.1	132.0	300.0	0.440

4. Extended investigation on eccentrically loaded CFDST columns

In this section, the behaviour of eccentrically loaded square CFDST columns with SHS inner tubes is evaluated. This is done based on the FE model validated in Section 2, but with a slight modification. The aim of this modification was to define the tensile strength and the softening behaviour of the concrete. This is because the concrete fill in beam-columns suffers from tensile stresses resulting from the bending moments. This has been made similar to that previously defined (and correctly validated) by the authors (Hassanein, et al. [29]) in their investigation of slender composite columns. Additionally, the damaged plasticity model has been utilised because the linear Drucker-Prager model is restricted to the concrete under compression only. Currently, loads at eccentricities of $\frac{B_o}{16}$, $\frac{B_o}{8}$, $\frac{B_o}{4}$ *and* $\frac{B_o}{2}$ are applied, producing a moment-interaction diagram for each group of specimens. In addition to the load-axial deflection curves, a series of moment-interaction diagrams was also produced for each specimen. Loads at eccentricities of 13.69 mm, 27.39 mm, 54.78 mm and 109.55 mm were applied to each specimen and combined with the concentric loading and pure bending cases to produce the diagrams. The FE results were compared with a theoretical model suggested by Han, et al. [30] and implemented by Tao, et al. [4]. This model is presented in the Appendix A.

It is worth pointing out that axial strength of the columns are indirectly compared with that calculated Han, et al. [30] during the comparisons between the FE and analytical interaction curves. Generally, the method of calculating the axial strength by Han, et al. [30] was found suitable, as can be noticed later on. On the other hand, as can be seen in the next sections presenting the effects of the eccentric loading considering each parameter previously examined in Section 3, the behaviour of the columns is well predicted by the theoretical model [4]. However, the shape of each curve fails to consistently match the curves produced from the FE models. Though, the trends identified from both sources are similar in each case.

4.1. Group 1: outer tube thickness

Fig. 17 (to the left) displays the moment-interaction curves of the four Group 1 specimens based on the FE models. It shows an appreciable reduction in both axial load and pure bending capacities as the slenderness ratio of the outer steel tube increases. This result is consistent with the load-axial deflection curves for Group 1 specimens, where it was found that the thickness of the outer steel tube has a significant effect on the overall behaviour of these short columns. The corresponding theoretical curves, as well, from Tao's model [4] are displayed in the same figure to the right. As expected, this model displays the considerable reduction in column capacity as the thickness of the outer steel tube decreases.

4.2. Group 2: inner tube thickness

The FE moment-interaction curves for the Group 2 specimens are presented in Fig. 18. The trend identified in this diagram again supports the results of the load-axial deflection graphs; the thickness of the inner steel tube reduces the ultimate axial capacity of the column, however, not as greatly as the outer steel tube. This finding can now be extended to the pure bending capacity of the column. Further support of this is shown in the theoretical curves in the right hand side of Fig. 18. This diagram shows very little variation in the behaviour of the column as the thickness of the inner steel tube is reduced, further supporting the findings of the FE models.

4.3. Group 3: hollow section ratio

Fig. 19 displays the moment-interaction curves of the Group 3 specimens. This series of curves presents a similar trend to that of the Group 2 specimens, where the behaviour of the columns changes negligibly across the four columns. As previously identified however, the strength-to-weight ratio of the columns drastically improves as the hollow section ratio increases, a benefit not displayed in the moment-interaction curves. Comparing the FE curves with the theoretical curves (in the same figure to the right) reveals a strong correlation in column behaviour as the hollow section ratio of the columns increase.

4.4. Group 4: concrete strength

The FE moment-interaction curves for the Group 4 specimens are presented in Fig. 20. As identified from the load-axial deflection curves, the concrete strength has a significant impact on the ultimate axial capacity of the columns as is to be expected. These results are further supported by the theoretical curves shown in Fig. 20.

4.5. Group 5: steel strength

The FE moment-interaction curves for the Group 5 specimens are presented in Fig. 21. Again this diagram presents a similar trend to that observed in the load-axial deflection curves. Increasing the strength of the steel markedly improves both the axial load and pure bending capacities of the column. This is further supported in Fig. 21(b), which

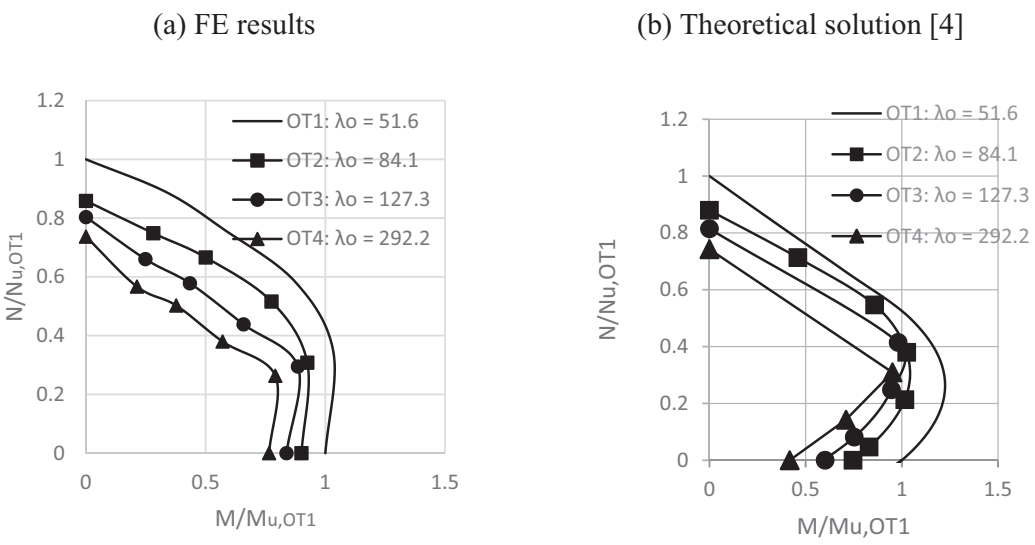

Fig. 17. Moment-interaction curves of Group 1 specimens: (a) FE results and (b) analytical solution [4].

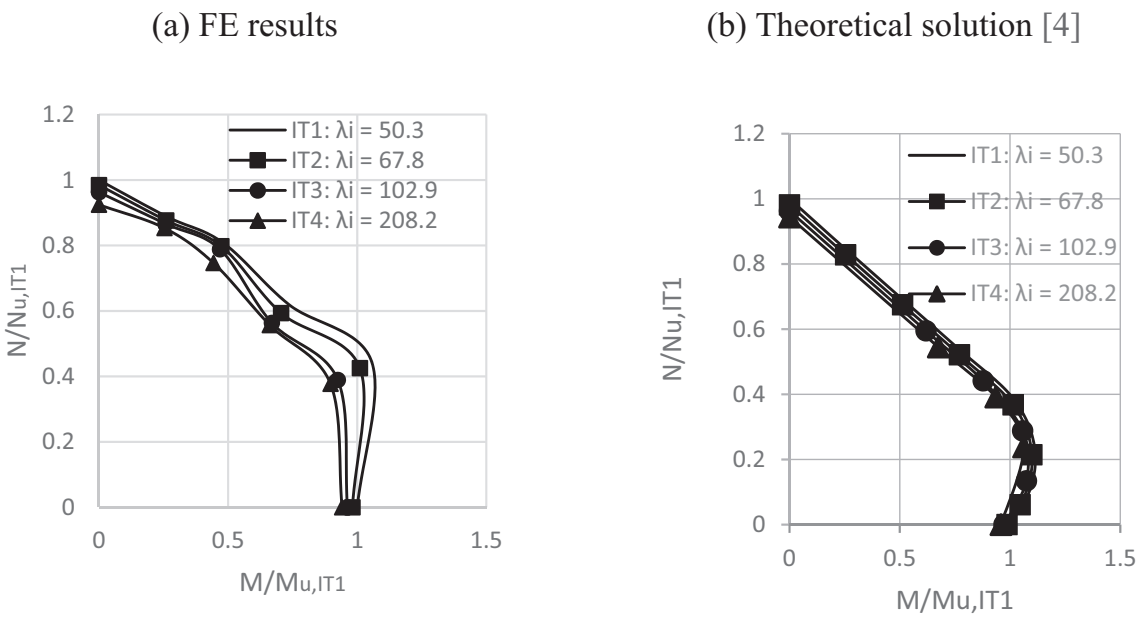

Fig. 18. Moment-interaction curves of Group 2 specimens: (a) FE results and (b) analytical solution [4].

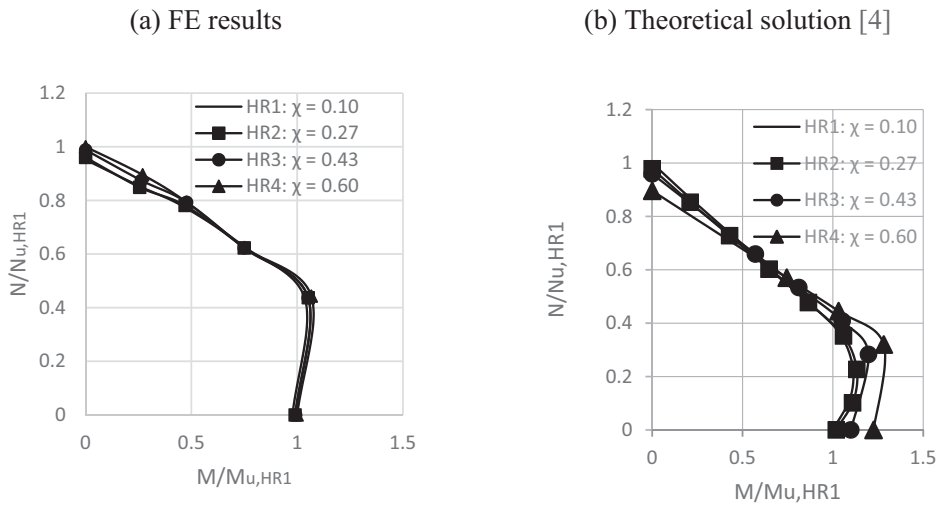

Fig. 19. Moment-interaction curves of Group 3 specimens: (a) FE results and (b) analytical solution [4].

displays the theoretical moment-interaction curves for the Group 5 specimens.

5. Summary and conclusions

A finite element (FE) analysis was performed on a series of CFDST columns with SHS outer and SHS inner steel tubes under both axial and eccentric loadings. This is to investigate the impact of changing six fundamental dimensional and material properties on the overall compressive behaviour of the column. Separate steel and concrete stress-strain models were used to predict the behaviour of the columns. These models were validated using the results of previous experiments, by ensuring the FE specimens could accurately replicate the load-axial deflection curves, maximum capacity and failure mechanisms of the experimental columns. It was found that the Ramberg-Osgood model for the steel tubes [2] and a model proposed by Zhao, et al. [11] for the concrete section, could produce accurate and reliable results for CFDST columns with SHS outer and SHS inner tubes. The three dimensional parameters investigated in the study were the slenderness ratio of the outer and inner steel tubes, the hollow section ratio as well as the material properties of the column. Four specimens with different properties were examined in each group.

- In Group 1, it was found that as the slenderness ratio of the outer tube was increased, the capacity of the column also declined. The reduction in weight of the columns was overshadowed by this reduction in capacity, meaning the strength-to-weight ratio of the columns declined as the thickness of the outer tube decreased.
- For the specimens in Group 2, the inner tube thickness was reduced. Across these four specimens, a similar trend to Group 1 of reduction in strength, albeit not as pronounced, was observed. The reduction in inner tube thickness was accompanied with a decline in column capacity and subsequent strength-to-weight ratio.
- The hollow section ratio was investigated in the Group 3 specimens. It was found that as the hollow ratio was increased from 0.1 to 0.6 across the four specimens, both the capacity and weight of the columns was improved. It was found from this group that increasing the hollow ratio was a highly effective way of improving the

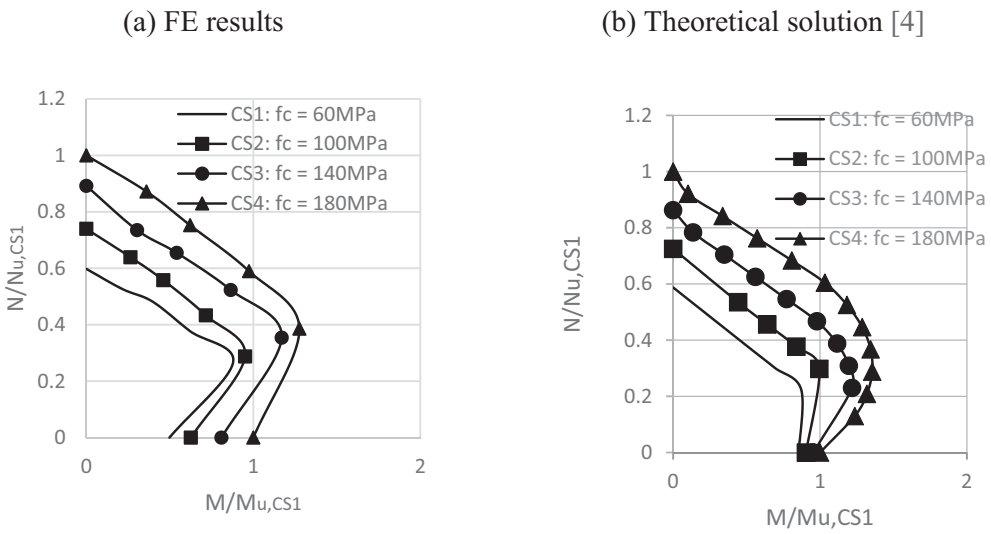

Fig. 20. Moment-interaction curves of Group 4 specimens: (a) FE results and (b) analytical solution [4].

strength-to-weight ratio of the CFDST column.

- Four specimens in Group 4 were used to examine the capacity of columns with concrete strength ranging from 60 MPa to 180 MPa. It was found that while the increased concrete strength brought about a greater column capacity, the process was only approximately 35% efficient. As well as this, the columns appeared to succumb to brittle failure which is highly unfavourable for construction purposes. The results of these tests indicate that increasing the concrete strength may not be a very effective method of improving the performance of CFDST columns.
- Group 5 was used to study the impact of the steel strength on the compressive capacity of the column. As expected, it was found that the steel strength greatly improved the capacity of the column. Again, this improvement was relatively inefficient however, with an increase in steel strength of 100% resulting in an overall increase in capacity of only 58.4%. This efficiency slumped even further when stronger steel was used. A positive outcome from this group of tests however, was the ductile nature in which the columns failed. This form of failure is desirable from a construction perspective.
- The axial strength model by Han, et al. [30] was found suitable for the current axially-loaded square CFDST columns with inner SHS tubes.
- The behaviour of the columns under eccentric loading was additionally examined. It was found that the columns' behaviour is well predicted by the theoretical model [4]. Though, the shape of each curve failed to consistently match the curves produced from the FE models, the trends identified from both sources are similar in each case.

Future investigation of CFDST columns with SHS outer and SHS inner tubes should be focused primarily on the dimensional parameters of the columns. The specimens tested in this paper identified that for a given column, increasing the slenderness ratios of the outer and inner steel tubes, resulted in a reduction in the strength-to-weight ratio of the column. Further investigation into this, either experimental or numerical, should determine the slenderness ratios of each tube which will optimise the strength-to-weight ratio of square CFDST columns. Similarly, further investigation to determine the optimal hollow section ratio for the strength-to-weight ratio of square CFDST columns would be highly beneficial. The specimens in this paper were tested with hollow ratios ranging from 0.1 to 0.6, however, hollow ratios up to 0.8 should also be studied.

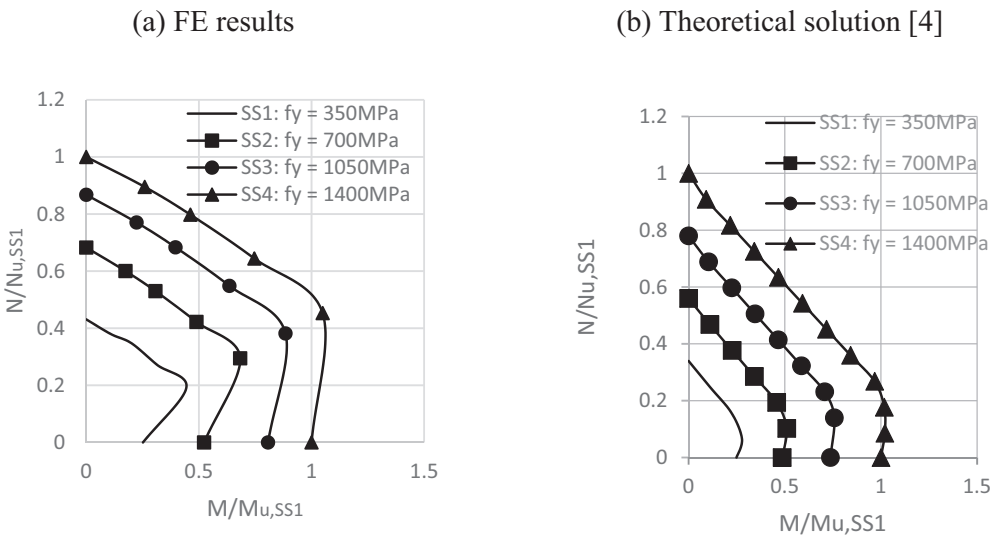

Fig. 21. Moment-interaction curves of Group 4 specimens: (a) FE results and (b) Analytical solution [4].

Appendix A. Interaction equations for columns suggested by Han, et al. (2003)

The axial load versus bending moment interaction curve of CFDST columns can be expressed as follows:

$$\frac{N}{\varphi N_u} + \frac{a}{d}\cdot\left(\frac{M}{M_u}\right) = 1 \quad (for N/N_u \geq 2\varphi^3\cdot\eta_o) \tag{A1a}$$

$$-\, b\cdot\left(\frac{N}{N_u}\right)^2 - c\cdot\left(\frac{N}{N_u}\right) + \frac{1}{d}\cdot\left(\frac{M}{M_u}\right) = 1 \quad (for N/N_u < 2\varphi^3\cdot\eta_o) \tag{A1b}$$

in which

$$a = 1 - 2\varphi^2\cdot\eta_o; \quad b = \frac{1-\varsigma_o}{\varphi^3\cdot\eta_o^2}; \quad c = \frac{2\cdot(\varsigma_o - 1)}{\eta_o}; \quad 1 - 0.4\cdot\left(\frac{N}{N_E}\right);$$

$$\varsigma_o = 1 + 0.18\xi^{-1.15};$$

$$\eta_o = \begin{cases} 0.5 - 0.2445\cdot\xi & (\xi \leq 0.4) \\ 0.1 + 0.14\cdot\xi^{-0.84} & (\xi > 0.4) \end{cases};$$

$$N_E = \frac{\pi^2\cdot E_{sc}^{elastic}\cdot A_{sc}}{\lambda^2} \tag{A1.1}$$

$E_{sc}^{elastic}$, which is the section modulus of CFDST in elastic stage, can be evaluated as:

$$E_{sc}^{elastic} = \frac{E_s(A_{so} + A_{si}) + E_c A_c}{A_{sc}} \tag{A1.2}$$

φ is the stability reduction factor, which is expressed as follows:

$$\varphi = \begin{cases} 1 & (\lambda \leq \lambda_o) \\ a_1\cdot\lambda^2 + b_1\cdot\lambda + c_1 & (\lambda_o < \lambda \leq \lambda_p) \\ \frac{d_1}{(\lambda+35)^2} & (\lambda > \lambda_p) \end{cases} \tag{A2}$$

where:

$$a_1 = \frac{1 + (35 + 2\cdot\lambda_p - \lambda_o)\cdot e_1}{(\lambda_p - \lambda_o)^2}; \quad b_1 = e_1 - 2\cdot a_1\cdot\lambda_p; \quad c_1 = 1 - a_1\cdot\lambda_o^2 - b_1\cdot\lambda_o;$$

$$d_1 = \left[13000 + 4657\cdot\ln\left(\frac{235}{f_{yo}}\right)\right]\cdot\left(\frac{25}{f_{ck}+5}\right)^{0.3}\cdot\left(\frac{\alpha}{0.1}\right)^{0.05}; \quad e_1 = \frac{-d_1}{(\lambda_p + 35)^3};$$

$$\lambda_o = \pi\cdot\sqrt{\frac{420\cdot\xi + 550}{f_{scy}}}; \quad \lambda_p = \pi\cdot\sqrt{250 + \frac{0.75E_s}{f_{yo}}} \tag{A2.1}$$

N_u, which is the axial load capacity of CFDST, can be determined as follows:

$$N_u = N_{osc,u} + N_{i,u} \tag{A3}$$

in which $N_{osc,\,u}$, the capacity of the outer steel tube with the sandwiched concrete, is determined by:

$$N_{osc,u} = A_{sco}\cdot f_{scy} \tag{A3.1}$$

where:

$$A_{sco} = A_{so} + A_c;$$
$$f_{scy} = C_1\chi^2\cdot f_{syo} + C_2(1.14 + 1.02\xi)\cdot f_{ck} \tag{A3.1.1}$$

f_{ck} is the characteristic concrete strength given by $f_{ck} = 0.67 f_{cu}$.f_{cu} is the characteristic cube strength of concrete.C_1 and C_2 are coefficients given by:

$$C_1 = \frac{\alpha}{(1+\alpha)}; \quad C_2 = \frac{(1 + \alpha_{nominal})}{(1+\alpha)} \tag{A3.1.2}$$

α is the steel ratio, and $\alpha_{nominal}$ is the nominal steel ratio, which can be determined as follows:

$$\alpha = \frac{A_{so}}{A_c}; \quad \alpha_{nominal} = \frac{A_{so}}{A_{c,nominal}} \tag{A3.1.3}$$

$N_{i,\,u}$ is the compressive capacity of the inner tube, and is given by:

$$N_{i,u} = A_{si}\cdot f_{yi} \tag{A3.2}$$

M_u, which is the bending moment capacity of CFDST, can be determined as follows:

$$M_u = \gamma_m W_{scm} f_{scy} + M_{i,u} \tag{A4}$$

where:

$$\gamma_m = 1.1 + 0.48\ln(\xi + 0.1); \quad W_{scm} = \frac{\pi(D_o^4 - B_i^4)}{32D_o} \tag{A4.1}$$

$M_{i,\,u}$ is the moment capacity of the inner tube, and is given by:

$$M_{i,u} = W_{si}.f_{yi} \tag{A4.2}$$

where W_{si} is the plastic section modulus of the inner tube.

Notations

Roman letters

A_c	Cross-sectional area of concrete
$A_{c,nominal}$	Nominal cross-sectional area of concrete.
A_{sc}	Cross-sectional area of the composite section
A_{sco}	Combined cross-sectional area of the outer steel tube and the sandwiched concrete
A_{si}	Cross-sectional area of the inner steel tube
A_{so}	Cross-sectional area of the outer steel tube
B	Width of a square column.
B_i	Width of the inner square steel column.
B_o	Width of the outer square steel column.
E_c	Elastic Modulus of concrete
E_s	Elastic Modulus of steel
f_c	Compressive strength of unconfined concrete
f_{cc}	Compressive strength of confined concrete
f_{ck}	Characteristic concrete strength
f_u	Ultimate strength of steel
f_y	Yield strength of steel
f_{yi}	Yield strength of the inner steel tube
f_{yo}	Yield strength of the outer steel tube
i	Radius of gyration of the CFDST column
I_{sc}	Moment of inertia for the CFDST column cross-section
L	Effective buckling length of the column in the plane of bending
M	Applied moment
$M_{i,u}$	Moment capacity of the inner steel tube
M_u	Ultimate moment capacity of the CFDST column
N	Applied axial force
$N_{i,u}$	Compressive capacity of the inner steel tube
N_u	Ultimate axial capacity of the CFDST column
$N_{osc,u}$	Compressive capacity of the outer steel tube and the sandwiched concrete
t	Thickness of a steel tube
t_i	Thickness of the inner steel tube
t_o	Thickness of the outer steel tube
W_{scm}	Plastic section modulus of the outer steel tube and sandwiched concrete
W_{si}	Plastic section modulus of the inner steel tube

Greek letters

α	Steel ratio
$\alpha_{nominal}$	Nominal steel ratio
ε	Strain value
ε_{cc}	Concrete strain value corresponding to f_{cc}
ε_{co}	Concrete strain value corresponding to f_c
ε_r	Strain of steel at rupture
λ	Column slenderness ratio
λ_s	Section slenderness ratio
ξ	Confinement factor
σ	Steel stress value
$\sigma_{concrete}$	Concrete stress value
χ	Hollow section ratio

References

[1] Han LH, Li W, Bjorhovde R. Developments and advanced applications of concrete-filled steel tubular (CFST) structures: members. J Constr Steel Res 2014;100:211–28.

[2] Elchalakani M, Karrech A, Hassanein MF, Yang B. Plastic and yield slenderness limits for circular concrete filled tubes subjected to static pure bending. Thin-Walled Struct 2016;109:50–64.

[3] Zhao X, Grzebieta R. Strength and ductility of concrete filled double skin (SHS inner and SHS outer) tubes. Thin-Walled Struct 2002;40:199–213.

[4] Tao Z, Han L-H, Zhao X-L. Behaviour of concrete-filled double skin (CHS inner and CHS outer) steel tubular stub columns and beam-columns. J Constr Steel Res 2004;60(1):1129–58.

[5] Han L-H, Tao Z, Huang H, Zhao X-L. Concrete-filled double-skin (SHS outer and CHS

inner) steel tubular beam-columns. Thin-Walled Struct 2004;42(9):1329–55.
[6] Elchalakani M, Zhao X-L, Grzebieta R. Tests on concrete filled double-skin (CHS outer and SHS inner) composite short columns under axial compression. Thin-Walled Struct 2002;40:415–41.
[7] Lu H, Zhao X-L, Han L-H. Testing of self-consolidating concrete-filled double skin tubular stub columns exposed to fire. J Constr Steel Res 2010;66:1069–80.
[8] Han L-H, Li Y-J, Liao F-Y. Concrete-filled double skin steel tubular (CFDST) columns subjected to long-term sustained loading. Thin-Walled Struct 2011;49:1534–43.
[9] Yang Y-F, Han L-H, Sun B-H. Experimental behaviour of partially loaded concrete filled double-skin steel tube (CFDST) sections. J Constr Steel Res 2012;71:63–73.
[10] Huang H, Han L-H, Tao Z, Zhao X-L. Analytical behaviour of concrete-filled double skin steel tubular (CFDST) stub columns. J Constr Steel Res 2010;66:542–55.
[11] Zhao X, Han B, Grzebieta R. Plastic mechanism analysis of concrete-filled double-skin (SHS inner and SHS outer) stub columns. Thin-Walled Struct 2002;40:815–33.
[12] Hassanein MF, Kharoob OF, Gardner L. Behaviour and design of square concrete-filled double skin tubular columns with inner circular tubes. Eng Struct 2015;100:410–24.
[13] Hassanein MF, Kharoob OF. Compressive strength of circular concrete-filled double skin tubular short columns. Thin-Walled Struct 2014;77:165–73.
[14] ABAQUS Standard, User's Manual. The Abaqus software is a product of Dassault Systèmes Simulia Corp., Providence, RI, USA Dassault Systèmes, Version 6.14, USA. 2014.
[15] Pagoulatou M, Sheehan T, Dai XH, Lam D. Finite element analysis on the capacity of circular concrete-filled double-skin steel tubular (CFDST) stub columns. Eng Struct 2014;72:102–12.
[16] Han LH, Yao GH, Tao Z. Performance of concrete-filled thin-walled steel tubes under pure torsion. Thin-Walled Struct 2007;45(1):24–36.
[17] Dai X, Lam D. Numerical modelling of the axial compressive behaviour of short concrete-filled elliptical steel columns. J Constr Steel Res 2010;66(7):931–42.
[18] Dai XH, Lam D, Jamaluddin N, Ye J. Numerical analysis of slender elliptical concrete filled columns under axial compression. Thin-Walled Struct 2014;77:26–35.
[19] Hassanein MF, Patel VI. Round-ended rectangular concrete-filled steel tubular short columns: FE investigation under axial compression. J Constr Steel Res 2018;140:222–36.
[20] Liu JP, Zhou XH, Gan D. Effect of friction on axially loaded stub circular tubed columns. Adv Struct Eng 2016;19(3):546–59.
[21] Zhou XH, Cheng GZ, Liu JP, Gan D, Chen YF. Behaviour of circular tubed-RC column to RC beam connections under axial compression. J Constr Steel Res 2017;130:96–108.
[22] AISC: American Institute of Steel Construction. Specification for structural steel buildings, ANSI/AISC 360-10. 2010.
[23] Yu T, Teng JG, Wong YL, Dong SL. Finite element modeling of confined concrete-I: Drucker-Prager type plasticity model. Eng Struct 2010;32:665–79.
[24] Richart FE, Brandtzaeg A, Brown RL. A study of the failure of concrete under combined compressive stresses. Bull. 185. Champaign (III): University of Illionis, Engineering Experimental Station; 1928.
[25] Hu H-T, Schnobrich W. Constitutive modelling of concrete by using nonassociated plasticity. J. Mater. Civil Eng 1989;1(4).
[26] Liang QQ. Performance-based analysis of concrete-filled steel tubular beam-columns, part I: theory and algorithms. J Constr Steel Res 2009;65:363–72.
[27] Jiao H, Zhao X-L, Lau A. Hardness and compressive capacity of longitudinally welded very high strength steel tubes. J Constr Steel Res 2015;114:405–16.
[28] Liew JYR, Xiong M, Xiong D. Design of concrete filled tubular beam-columns with high strength steel and concrete. Structure 2012;8(2):213–26.
[29] Hassanein MF, Elchalakani M, Patel VI. Overall buckling behaviour of circular concrete-filled dual steel tubular columns with stainless steel external tubes. Thin-Walled Structures 2017;115:336–48.
[30] Han L, Yao G, Tao Z, Yang Y. Series study and design of concrete-filled HSS columns subjected to different kind of loading states. Fuzhou: College of Civil Engineering and Architecture; 2003.